processes

MDPI

Article

Unsteady Natural Convection in an Initially Stratified Air-Filled Trapezoidal Enclosure Heated from Below

Md. Mahafujur Rahaman [1,2], Sidhartha Bhowmick [1], Rabindra Nath Mondal [1] and Suvash C. Saha [3,*]

[1] Department of Mathematics, Jagannath University, Dhaka 1100, Bangladesh; mahfuz0809@gmail.com (M.M.R.); sidharthabhowmick@yahoo.com (S.B.); rnmondal71@yahoo.com (R.N.M.)
[2] Department of Computer Science and Engineering, Z. H. Sikder University of Science and Technology, Shariatpur 8024, Bangladesh
[3] School of Mechanical and Mechatronic Engineering, University of Technology Sydney, Ultimo, NSW 2007, Australia
* Correspondence: suvash.saha@uts.edu.au

Abstract: Natural convection is intensively explored, especially in a valley-shaped trapezoidal enclosure, because of its broad presence in both technical settings and nature. This study deals with a trapezoidal cavity, which is initially filled with linearly stratified air. Although the sidewalls remain adiabatic, the bottom wall is heated, and the top wall is cooled. For the stratified fluid (air), the temperature of the fluid adjacent to the top and the bottom walls is the same as that of the walls. Natural convection in the trapezoidal cavity is simulated in two dimensions using numerical simulations, by varying Rayleigh numbers (Ra) from 10^0 to 10^8 with constant Prandtl number, Pr = 0.71, and aspect ratio, A = 0.5. The numerical results demonstrate that the development of natural convection from the beginning is dependent on the Rayleigh numbers. According to numerical results, the development of transient flow within the enclosure owing to the predefined conditions for the boundary may be categorized into three distinct stages: early, transitional, and steady or unsteady. The flow characteristics at each of the three phases and the impact of the Rayleigh number on the flow's growth are quantified. Unsteady natural convection flows in the enclosure are described and validated by numerical results. In addition, heat transfer through the bottom and the top surfaces is described in this study.

Keywords: stratified air; trapezoidal cavity; natural convection; heat transfer; transient flow

Citation: Rahaman, M.M.; Bhowmick, S.; Mondal, R.N.; Saha, S.C. Unsteady Natural Convection in an Initially Stratified Air-Filled Trapezoidal Enclosure Heated from Below. *Processes* **2022**, *10*, 1383. https://doi.org/10.3390/pr10071383

Academic Editor: Iztok Golobič

Received: 22 June 2022
Accepted: 12 July 2022
Published: 15 July 2022

1. Introduction

In an enclosure, natural convection has gained substantial interest among academics since it can be found in a variety of applications and has a big impact on thermal characteristics. Natural convection has been studied inside various shapes of enclosures with numerous boundary conditions to investigate thermal behavior, as well as fluid flow, as natural convection is used in an array of technical applications, ranging from geophysics, geothermal reservoirs, and building insulation to industrial separation processes and so forth. Unsteady natural convection in a differentially heated cavity has attracted extensive attention in the scientific literature. Many researchers [1–6] provided comprehensive investigations for regular enclosures (e.g., rectangular, square and triangular) using various numerical models, indicating that multiple investigations have been performed to gain a fundamental understanding of unsteady natural convection flows and heat transfer characteristics in an enclosure.

Due to the importance of attics for occupant thermal comfort in buildings and the resulting energy costs for heating and air conditioning, increased research activities have been carried out on subjects related to heat transfer in attics over the last 40 years. Saha et al. [7,8] examined heat transport through attics under periodic thermal forcing and cooling inclined

walls. Natural convection flows within V-shaped triangle enclosures with opposite boundary conditions appeared to be well studied due to their natural presence. Transitions from symmetric steady to asymmetric unsteady flow were studied by Bhowmick et al. [9,10] in a V-shaped triangular enclosure heated from below and cooled from the top for both air and water. Different flow mechanisms were found for the different fluids. Wang et al. [11] has experimented with natural convection in a V-shaped enclosure with the same boundary conditions of [10].

Any triangular, square, or rectangular cavity is inadequate for numerous engineering systems, as well as geophysical circumstances where the enclosure geometry varies or contains extra tending walls. Natural convection in a trapezoidal enclosure is far more difficult to examine than in any regular enclosures because of the sloped walls. This complicated geometry needs a precise and large effect in mesh creation and code development. However, there were a number of studies on natural convection that focused on trapezoidal enclosures. Iyican et al. [12,13] considered trapezoidal cavity with boundary conditions of a heated base wall and parallel cylindrical cooled top wall to investigate natural convection of the cavity, using experimental and computational methods. Lee [14] reported a theoretical and experimental investigation of a nonrectangular enclosure, in which two 45° inclined sides of a trapezoidal cross-section were chosen, with different heating conditions. Lam et al. [15] found analogous findings for a trapezoidal enclosure with cooled inclined top wall, heated bottom wall, and insulated vertical sidewalls.

Lee [16] numerically examined the fluid flow and the heat transfer passed through a cold chamber of a trapezoidal enclosure, where heated fluid was supposed to flow into one end of the chamber from a depth below the surface and was removed from the other end at a different depth. Lee [17] and Peri [18] showed numerical findings in the case of laminar natural convection within a trapezoidal cavity with inclined sidewalls kept at varying constant temperatures, and adiabatic top and base walls for $Ra \leq 10^6$. Sadat and Salagnac [19] used a finite element based on the control-volume approach to compute the similar geometry for Rayleigh numbers from 10^3 to 2×10^5. Kuyper and Hoogendoorn [20] examined laminar natural convection flow within a trapezoidal cavity in order to see the effect of the flow by the inclination angle, as well as the relationship between the Ra and the average Nu. Moukalled and Darwish [21] looked at how heat transfer was affected by installing baffles upon the top inclined walls inside trapezoidal cavities. Boussaid et al. [22] examined thermal heat transfer inside a trapezoidal chamber in which the base wall was heated and the tending upper half was cooled. The influence of natural convection flow within a trapezoidal cavity was examined by Natarajan et al. [23] under the conditions of a heated base wall, as well as linearly heated and cooled vertical walls, but with no insulation on the top wall. Hammami et al. [24] investigated the fixed heat and mass transport processes within a trapezoidal enclosure using a binary air–water vapor mixture. Later, Natarajan et al. [25] explored natural convection flow inside a trapezoidal cavity in which, on the one hand, the base wall was both consistently and inconsistently warmed, and the upward walls were, through a steady temperature shower, kept cool, where the upper wall again remained insulated. Basak et al. [26] examined natural convection energy fluxes in trapezoidal enclosures in which the top walls were insulated, whereas the bottom walls were heated, and sidewalls were cooled.

For three vertex angles in trapezoidal isosceles, the advancement of natural convection oscillatory flow patterns was examined by Noah and Daniel [27]. Mustafa and Ghani [28] explored a natural convection flow inside a trapezoidal cavity with partially heated bottom wall and cooled vertical walls through a constant temperature bath and a well-insulated top wall. By means of the 'element-based finite volume method', Silva et al. [29] studied natural convection inside trapezoidal enclosures. Gholizadeh et al. [30] explored the natural convection inside a trapezoidal enclosure where the right inclined wall was partially heated, by means of the finite difference method. In a porous trapezoidal enclosure saturated through a power-law non-Newtonian fluid, Yazdani et al. [31] considered natural convection, as well as entropy production. To better comprehend the effect of heating

length on the active bottom wall, Gowda et al. [32] observed natural convection within the cavity of a trapezoid under the condition that the base wall was partly heated, the upper wall was adiabatic, and the inclined wall remained at a fixed cooled temperature.

Various boundary conditions were used in the trapezoidal cavity by various researchers, according to the above literature studies. However, an initially stratified air-filled trapezoidal enclosure with a cooled top horizontal wall and a heated bottom horizontal wall, along with inclined walls that are kept adiabatic, is still ambiguous, which encouraged this research. It has direct application to environmental fluid dynamics, which deals with the heat transfer and airflow process in the thermal stratification environment. Thus, using two-dimensional numerical simulations for Ra = 10^0 to 10^8, Pr = 0.71, and A = 0.5, the transitional flow in the trapezoidal cavity is considered in this article. The influence of Ra on fluid flow and heat transfer is thoroughly examined.

2. Problem Formulations

This study considers a trapezoidal enclosure of height H, as well as a horizontal length of the top, $2L$, where $L = 2H$, i.e., $A = H/L = 0.5$. Figure 1 illustrates a nondimensional physical model with boundary conditions. A tiny percentage (4% of L) of each top corner was sliced to dispense with the singularity around the position between inclination and upper walls, and cutting walls were subject to an adiabatic thermal state. A fluid in the cavity with Pr = 0.71 was considered, which was, in the beginning, linearly stratified as having the highest $T = T_h$ temperature at the bottom and the lowest $T = T_c$ temperature at the top. The boundaries were non-slip.

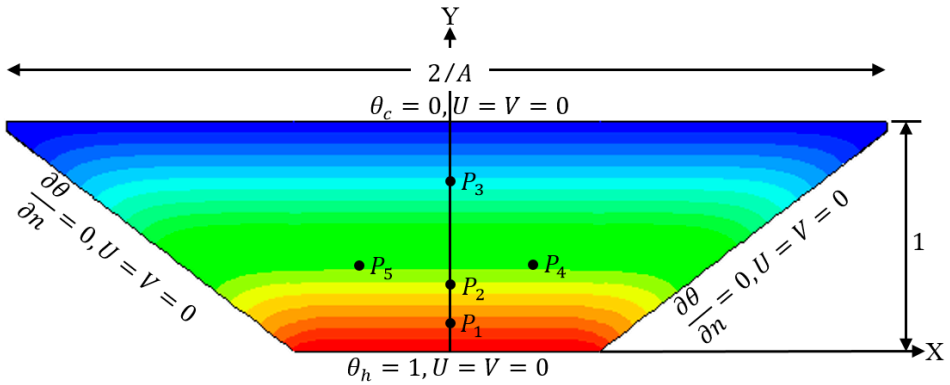

Figure 1. Schematic of physical domain with nondimensional boundary conditions with the monitoring points P_1 (0, 0.133), P_2 (0, 0.4), P_3 (0, 0.8), P_4 (0.4, 0.51), and P_5 (−0.4, 0.51), which are utilized in the resulting figures.

In a trapezoidal enclosure, natural convection of stratified air is assumed. The below set of governing equations with the Boussinesq approximation regulates the progress of natural convection flows in the enclosure [7].

$$\frac{\partial u}{\partial x} + \frac{\partial v}{\partial y} = 0, \tag{1}$$

$$\frac{\partial u}{\partial t} + u\frac{\partial u}{\partial x} + v\frac{\partial u}{\partial y} = -\frac{1}{\rho}\frac{\partial p}{\partial x} + \nu\left(\frac{\partial^2 u}{\partial x^2} + \frac{\partial^2 u}{\partial y^2}\right), \tag{2}$$

$$\frac{\partial v}{\partial t} + u\frac{\partial v}{\partial x} + v\frac{\partial v}{\partial y} = -\frac{1}{\rho}\frac{\partial p}{\partial y} + \nu\left(\frac{\partial^2 v}{\partial x^2} + \frac{\partial^2 v}{\partial y^2}\right) + g\beta(T - T_0), \tag{3}$$

$$\frac{\partial T}{\partial t} + u\frac{\partial T}{\partial x} + v\frac{\partial T}{\partial y} = \kappa\left(\frac{\partial^2 T}{\partial x^2} + \frac{\partial^2 T}{\partial y^2}\right). \tag{4}$$

The followings are the dimensionless variables that were used:

$$\begin{aligned} X &= \tfrac{x}{H}, \\ Y &= \tfrac{y}{H}, \\ U &= \tfrac{uH}{\kappa \mathrm{Ra}^{1/2}}, \\ V &= \tfrac{vH}{\kappa \mathrm{Ra}^{1/2}}, \\ P &= \tfrac{pH^2}{\rho \kappa^2 \mathrm{Ra}}, \\ \theta &= \tfrac{T-T_\infty}{T_h-T_c}, \\ \tau &= \tfrac{t\kappa \mathrm{Ra}^{1/2}}{H^2}. \end{aligned} \tag{5}$$

The three governing parameters, which are aspect ratio (A), Pr, and Ra (see Ref. [33] for details), influence the natural convective flows in the enclosure that can be expressed as follows:

$$\mathrm{Ra} = \frac{g\beta(T_h - T_c)H^3}{\nu\kappa}, \ \mathrm{Pr} = \frac{\nu}{\kappa}, \ A = \frac{H}{L}. \tag{6}$$

After adding the aforementioned dimensionless variables, Equations (1)–(4) become (for details see Ref. [10])

$$\frac{\partial U}{\partial X} + \frac{\partial V}{\partial Y} = 0, \tag{7}$$

$$\frac{\partial U}{\partial \tau} + U\frac{\partial U}{\partial X} + V\frac{\partial U}{\partial Y} = -\frac{\partial P}{\partial X} + \frac{\mathrm{Pr}}{\mathrm{Ra}^{1/2}}\left(\frac{\partial^2 U}{\partial X^2} + \frac{\partial^2 U}{\partial Y^2}\right), \tag{8}$$

$$\frac{\partial V}{\partial \tau} + U\frac{\partial V}{\partial X} + V\frac{\partial V}{\partial Y} = -\frac{\partial P}{\partial Y} + \frac{\mathrm{Pr}}{\mathrm{Ra}^{1/2}}\left(\frac{\partial^2 V}{\partial X^2} + \frac{\partial^2 V}{\partial Y^2}\right) + \mathrm{Pr}\theta, \tag{9}$$

$$\frac{\partial \theta}{\partial \tau} + U\frac{\partial \theta}{\partial X} + V\frac{\partial \theta}{\partial Y} = \frac{1}{\mathrm{Ra}^{1/2}}\left(\frac{\partial^2 \theta}{\partial X^2} + \frac{\partial^2 \theta}{\partial Y^2}\right). \tag{10}$$

3. Timestep and Grid Dependency Tests

In this study, ANSYS FLUENT 17.0, a finite-volume-based fluid simulation software, was used to enable the high Rayleigh number flows (Armfield and Street [34–36]). In order to find solutions to the governing Equations (7)–(10) and other conditions, the SIMPLE scheme was used. Using the QUICK scheme (see Leonard and Mokhtari [37]), the advection term was discretized. Central differencing, along with second-order accuracy, was used to discretize the diffusion terms. Moreover, a second-order implicit time-marching scheme was employed for the unsteady term.

The grid and timestep dependency tests were also performed for the greatest Rayleigh number, Ra = 10^8, used in this study. Three symmetrical meshes of 225 × 75, 300 × 100, and 375 × 125 were created nonuniformly using the application ANSYS ICEM, by way of coarser grids in the interior area and finer grids around the edges. From a width of at least 0.002 adjacent to the wall to the width of 0.02 in the interior, the mesh of 300 × 100 was increased at a rate of 3%. At position P_2 (0, 0.4), employing various grids together with timesteps, the temperature timeseries was computed for Ra = 10^8 as depicted in Figure 2. The results evidently show that temperatures predicted with various meshes and timesteps were constant in the initial phases, but somewhat deviated in the fully developed stage.

Table 1 shows the maximum variation of the average temperature at the fully developed stage for the different meshes and timesteps. The highest contrast of the temperature between the coarsest (225 × 75) and finest (300 × 100) meshes was around 1.42%, while the highest difference between the finer meshes (300 × 100) and (375 × 125) was approximately

0.34%. Therefore, considering the computational cost, a mesh of 300 × 100 and a timestep of 0.01 were used in the numerical simulation.

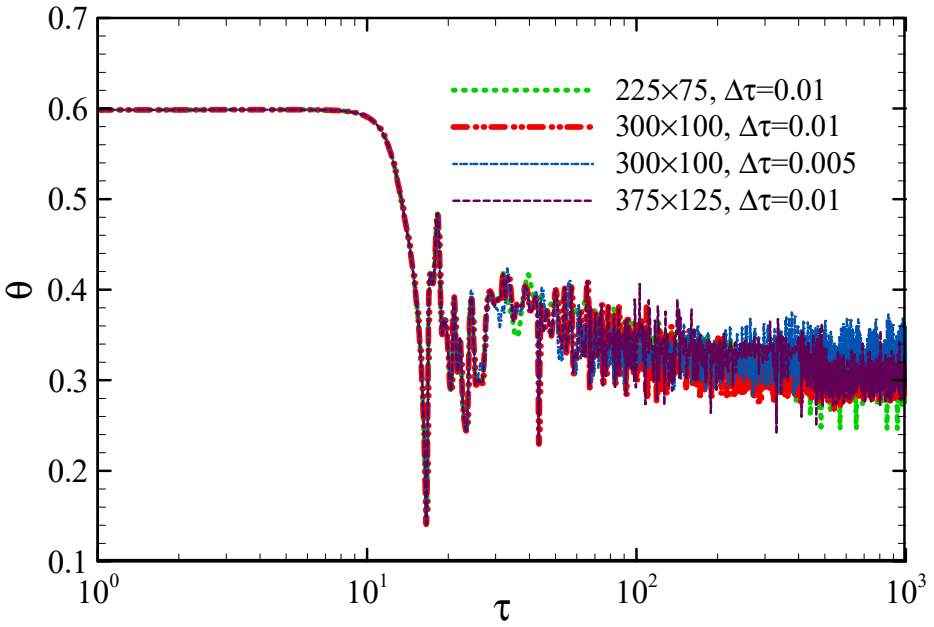

Figure 2. Temperature time series at P_2 (0, 0.4) for Ra = 10^8 with distinct grids and timesteps.

Table 1. Temperature at P_2 (0, 0.4) employing various grids and timesteps.

Grids and Time Steps	Average Value of the Temperature	Percentage of the Variance
225 × 75 and Δτ = 0.01	0.306495	1.42%
300 × 100 and Δτ = 0.01	0.310895	-
300 × 100 and Δτ = 0.005	0.313003	0.68%
375 × 125 and Δτ = 0.01	0.309845	0.34%

4. Validation

Validation of a model is an integral part of a numerical study. Hence, the numerical results of the present study were compared to those of Basak et al. [26], who used the finite element method to solve the governing equations for laminar natural convection heat transfer in a trapezoidal cavity heated isothermally from below, while maintaining a fixed cold temperature on the other vertical walls and a well-insulated top wall. With Ra = 10^5, Pr = 0.71, and an inclination angle of φ = 45°, the dimensionless parameters were used to conduct the comparison. The current findings and the numerical findings of Basak et al. [26] for temperature contours in the trapezoidal enclosure exhibited excellent agreement, as shown in Figure 3.

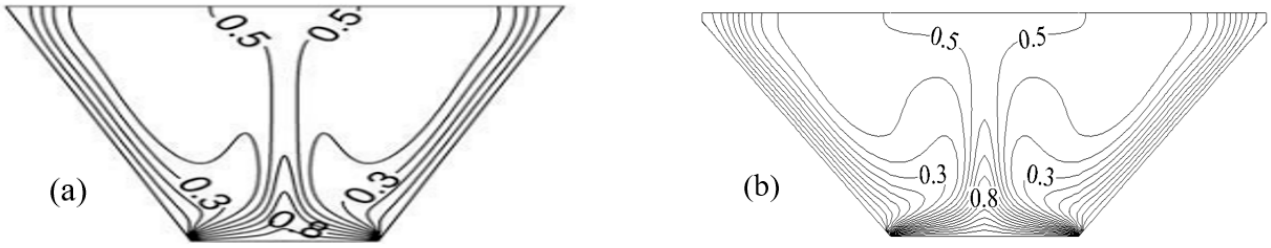

Figure 3. Comparison of the results of Basak et al. [26]: (**a**) the present study; (**b**) for the temperature contours in the trapezoidal enclosure where Ra = 10^5, Pr = 0.7, and inclination angle φ = 45°.

5. Results and Discussions

For Ra = 10^0 to 10^8, Pr = 0.71, and A = 0.5, the transient evolution of the flow in an initially stratified air-filled trapezoidal cavity is discussed below in response to consistent heating through the base and similar cooling via the top surfaces using a computational fluid dynamics approach.

5.1. Development of the Transient Flow

For Ra = 10^0 to 10^2, it was found that there was no ascending or descending plume in the flow development, i.e., the flow was always steady under a conduction dominance for those Rayleigh numbers. For the sake of brevity, results are not presented here for Ra = 10^0 to 10^2. Accordingly, for Ra = 10^3 to 10^8, the general characteristics of flow development in a trapezoidal enclosure are presented (see Figures 4–6). The development of the flow for these Rayleigh numbers, according to the numerical simulations, may be divided into the following: early stage, transitional stage, and steady or unsteady stage.

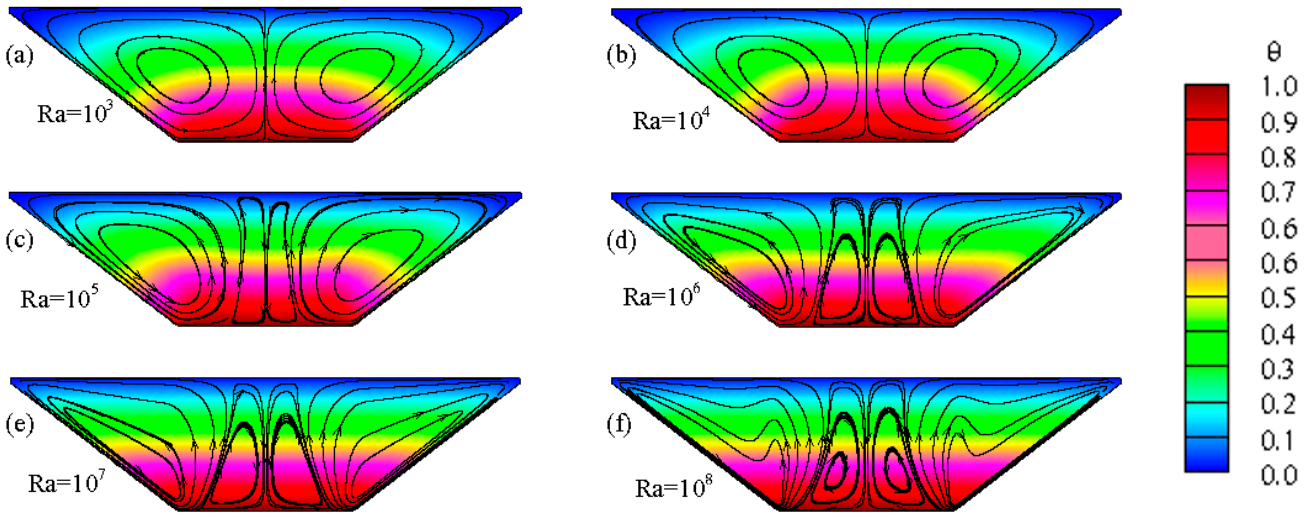

Figure 4. Streamlines and isotherms at the early stage for the different Rayleigh numbers (**a**) Ra = 10^3, (**b**) Ra = 10^4, (**c**) Ra = 10^5, (**d**) Ra = 10^6, (**e**) Ra = 10^7, (**f**) Ra = 10^8, at τ = 6.

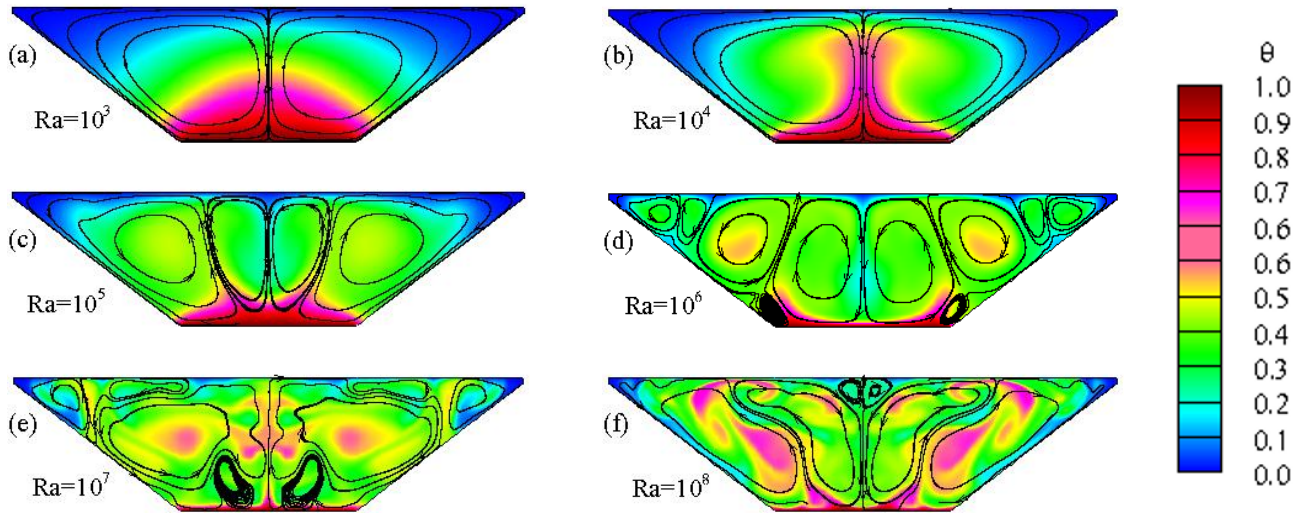

Figure 5. Streamlines and isotherms at the initial transitional stage for the different Rayleigh numbers (**a**) Ra = 10^3, (**b**) Ra = 10^4, (**c**) Ra = 10^5, (**d**) Ra = 10^6, (**e**) Ra = 10^7, (**f**) Ra = 10^8, at τ = 20.

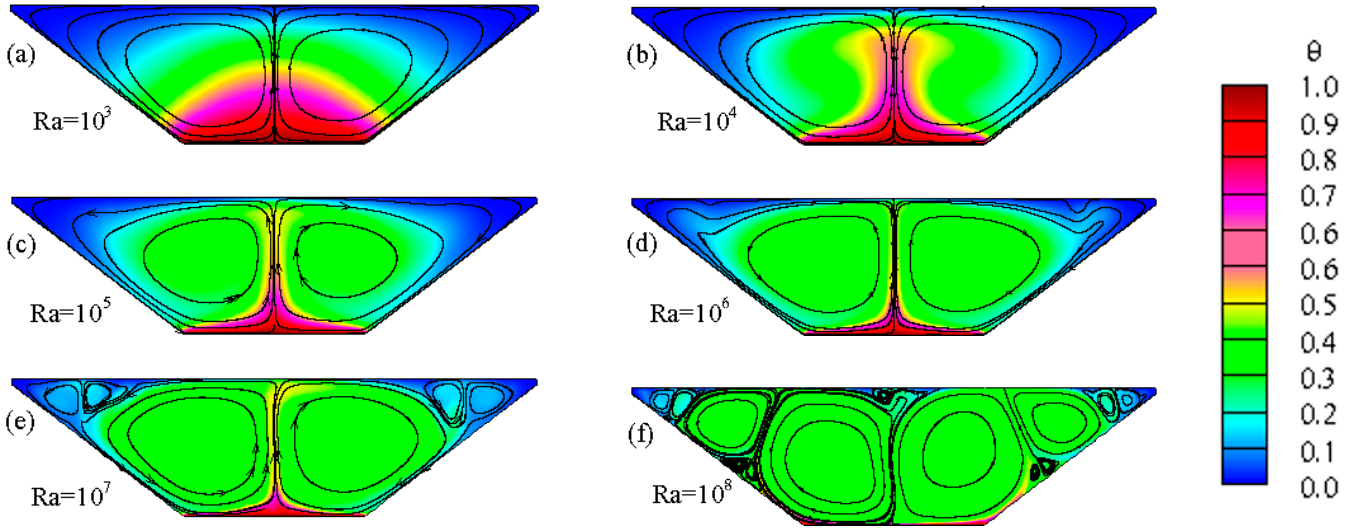

Figure 6. Streamlines and isotherms at the developed transitional stage for the different Rayleigh numbers (**a**) Ra = 10^3, (**b**) Ra = 10^4, (**c**) Ra = 10^5, (**d**) Ra = 10^6, (**e**) Ra = 10^7, (**f**) Ra = 10^8, at τ = 100.

5.1.1. Flow at the Early Stage

In the trapezoidal enclosure, the air is at first stratified, as indicated in the preceding sections. At the beginning of the numerical studies, the instant conditions for isotherms are created across the surfaces that first cool the cavity via the upper surface and then make it warm through the bottom. A thermal boundary layer forms along all internal surfaces as a result. The cooling thermal boundary layer is near the top wall, whereas the heating thermal boundary layer is alongside the bottom surface. The lower section produces the heating thermal boundary layer, while the top section of the upper layer produces the cooling thermal boundary layer. The progress of the thermal boundary layers through time is depicted in Figure 4, exhibiting isotherms and streamlines (Figure 4a–e) at τ = 6 after startup.

At the early stage, the core's fluid stays isothermal, as shown in Figure 4, in spite of the expansion of the thermal boundary layer, at the initial temperature. Because the bottom part of the enclosure is heated and the top section is cooled, the heated fluid from the bottom travels via the boundary layer toward the upper parts. On the contrary, the boundary layer transports cooled air to the bottom from the top. Both warm and cold fluids meet in the middle of the top wall and release into the core. There remains another heated boundary layer near the bottom section that begins to expand, as the thermal forcing begins. At this moment, the isothermal difference reveals the thicknesses of the thermal layer barrier to the center growing with time. The streamlines show that Ra = 10^3 to 10^5 has two weak revolving cells, while Ra = 10^6 to 10^8 has four weak rotating cells. The isotherms and streamlines for different Ra remain symmetric with regard to the cavity's *y*-axis line at this stage.

5.1.2. Transitional Stage

The formation of convective instabilities marks the flow in the form of ascending and descending plumes at the transitional phase. Through the warming of the bottom portion, the horizontal thermal boundary layer, which has warmed air under colder air and is unstable due to 'Rayleigh–Bénard instabilities', is formed. When the critical conditions are fulfilled, the hot thermal boundary layer becomes unsteady. In this regime, Figures 5 and 6 display the streamlines and isotherms at various periods. It has previously been noted that when air of two different temperatures passes through the boundary layer around the midpoint of inclined surfaces, it invariably travels downward. Subsequently, the heated air plume then moves to the cavity's core, while the cooled air plume goes to the lower

portion from the upper layer. Figure 5a,b show that the flow becomes symmetric and steady at $\tau = 20$ for Ra = 10^3 to 10^4. The flow grows stronger and finally asymmetric as time passes due to pitchfork bifurcation. The figures demonstrate the asymmetric isotherms and streamlines for the higher Rayleigh numbers. It is without a doubt significant that, with a greater Rayleigh number, the flow oscillates for quite a long period. The bifurcation continues to rehash left and close to the symmetric focal line while oscillating. Figure 6c,d depict that the flow becomes symmetric and steady at $\tau = 100$ for Ra = 10^5 to 10^6. Because of the presence of convective instabilities, the rotating cells that are at the beginning of the growth of the flow are fragmented into several cells, which is demonstrated in Figures 5 and 6 by the outlines of the isotherms and streamlines.

A pitchfork bifurcation starts to happen as a result of Rayleigh–Bénard instability. The x-velocity at point P_3 (0, 0.8) in the Ra-u plane is provided in Figure 7 to explain such a pitchfork bifurcation from the symmetric to asymmetric state at the completely developed stage ($\tau = 1000$). Because the flow is symmetric around the y-axis and point P_3 is on the y-axis, the x-velocity for Ra < 10^5 is close to zero. When the Rayleigh number surpasses or becomes equivalent to 10^5, the cell inclines to the right side with an increment in the x-velocity, as set apart by the square line, whereas it inclines to the left side with the reduction in x-velocity, as set apart by the blue line (circles) in Figure 7.

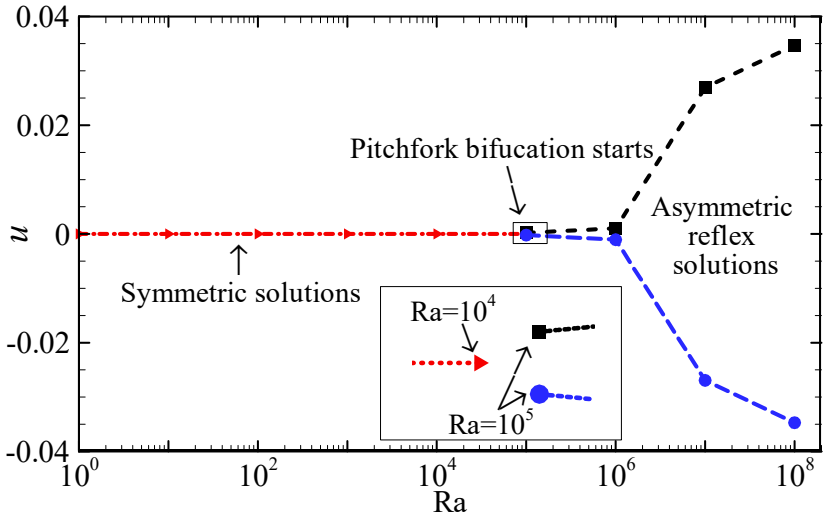

Figure 7. Pitchfork bifurcation in the Ra-u plane where u is the x-velocity at the point P_3 (0, 0.8).

5.1.3. Flow at the Steady or Unsteady Stage

In the late transitional phase, a pitchfork bifurcation occurs, resulting in the formation of an asymmetric flow structure. The pitchfork bifurcation occurs early in the numerical simulation, as previously mentioned.

The convective instabilities alternate on either side of the cavity, and the upward-moving heated air plumes on the base side appear in the middle at different times, which is a fascinating event as shown in the numerical simulation. During the transitional stage, the flow, on the other hand, has multiple undershoots and overshoots prior to becoming completely stable. Thermal energy travels from the boundary layer on either side of the portion discharge fluid to the cavity's center over time. At the fully developed phase, the fluid inside the enclosure reaches a steady state for Ra = 10^3 to 10^6 (see Figure 8a–d). If Ra $\leq 10^6$, Figure 8a–d reveal that the flow becomes stable under various initial conditions. Furthermore, for Ra $\geq 10^7$, Figure 8e,f depict isotherms and streamlines. Figure 8e represents a few tiny cells forming on the top right and left sides of the larger cell. However, when looking at the numerical data, it can be seen that the two tiny cells alternately emerge, indicating that the flow arrives in an unsteady state at a fully advanced stage for Ra = 10^7. With the increase in Ra, however, both cells develop in the center of the two biggest cells,

as seen in Figure 8f. In Figure 8f, for Ra = 10^8, the biggest cell in the center also travels between right and left. As a result, the unsteady flow becomes more complicated.

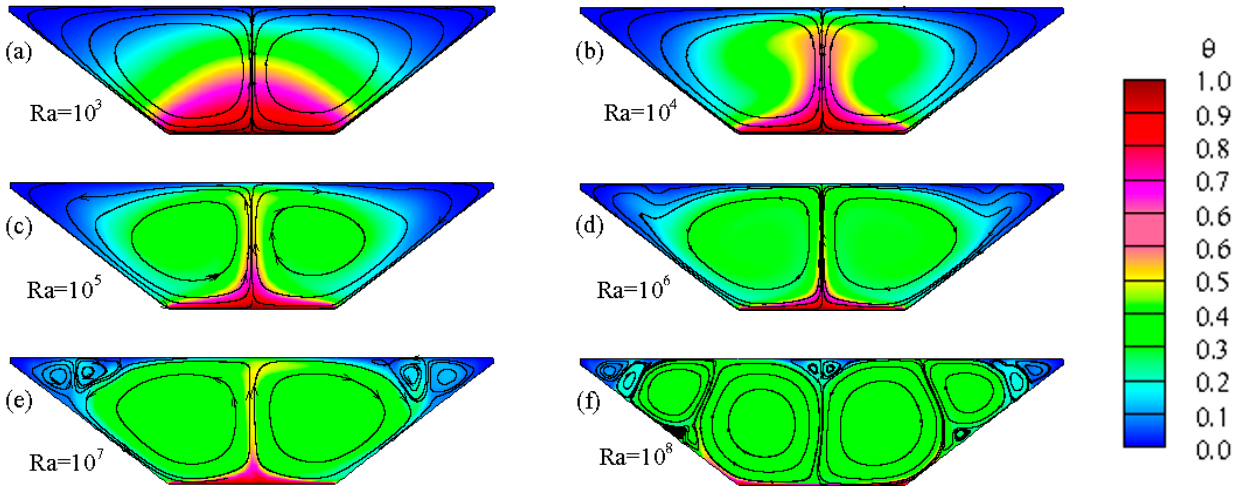

Figure 8. Streamlines and isotherms at the fully developed stage for the different Rayleigh numbers (**a**) Ra = 10^3, (**b**) Ra = 10^4, (**c**) Ra = 10^5, (**d**) Ra = 10^6, (**e**) Ra = 10^7, (**f**) Ra = 10^8, at τ = 2000.

To comprehend the unstable flow for greater Rayleigh numbers, a temperature–time series is presented in Figure 9. It is apparent that, at the completely advanced stage, the flow is stable, as shown in Figure 9a, and the flow pattern in Figure 9b concurs with the finding of a Hopf bifurcation from a steady state to periodic condition. With the increase in Ra, the periodic flow fluctuates, while the unstable flow becomes chaotic for Ra = 10^8. This is illustrated in Figure 9c.

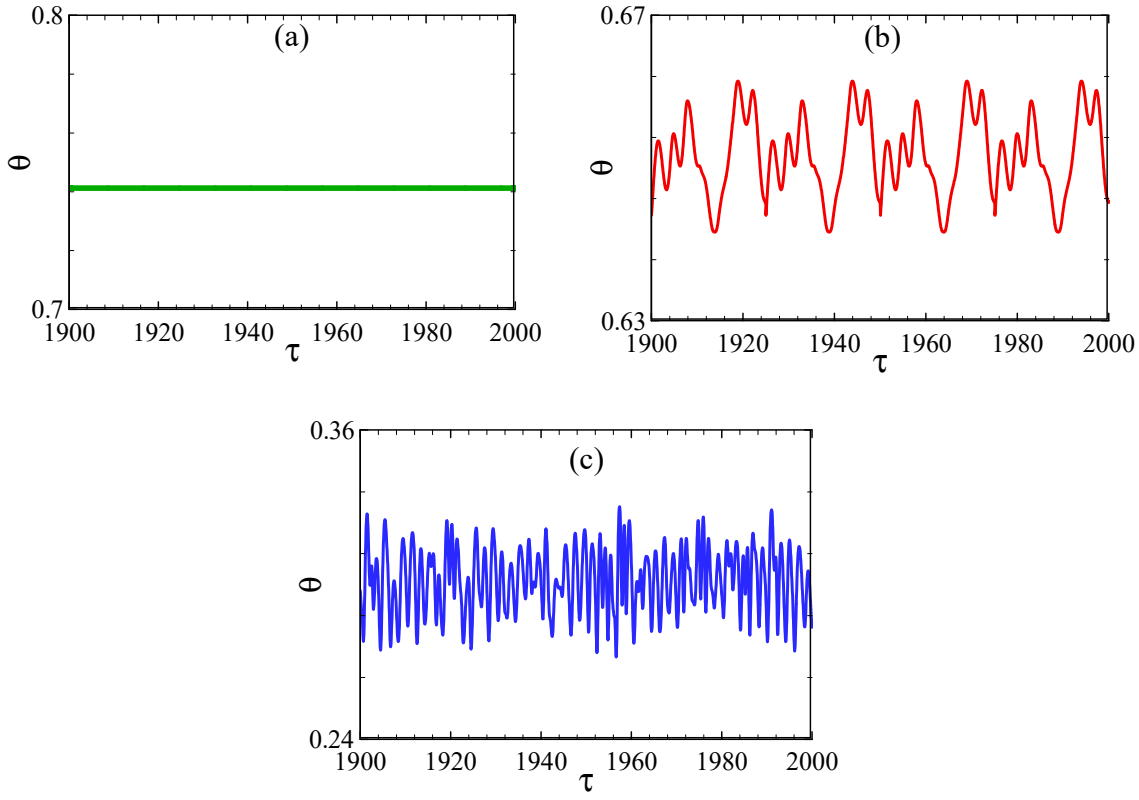

Figure 9. At the fully developed stage, temperature timeseries at point P_3 (0, 0.8) for (**a**) Ra = 10^6, (**b**) Ra = 10^7, and (**c**) Ra = 10^8.

To comprehend the Hopf bifurcation, which occurs at the transition from steady to periodic phase, the attractors (τ = 300 to 2000) for Ra = 10^6 and (τ = 1000 to 2000) for Ra = 10^7 at the point P_4 (0.4, 0.51) are depicted in Figure 10. In Figure 10a, the curve in the u–θ plane clearly approaches a certain value with the passage of time for Ra = 10^6. In contrast, Figure 10b shows a limit cycle for Ra = 10^7 (dense curve). Consequently, a Hopf bifurcation occurs at Ra = 10^7 (referred to [38] for a full description of Hopf bifurcation).

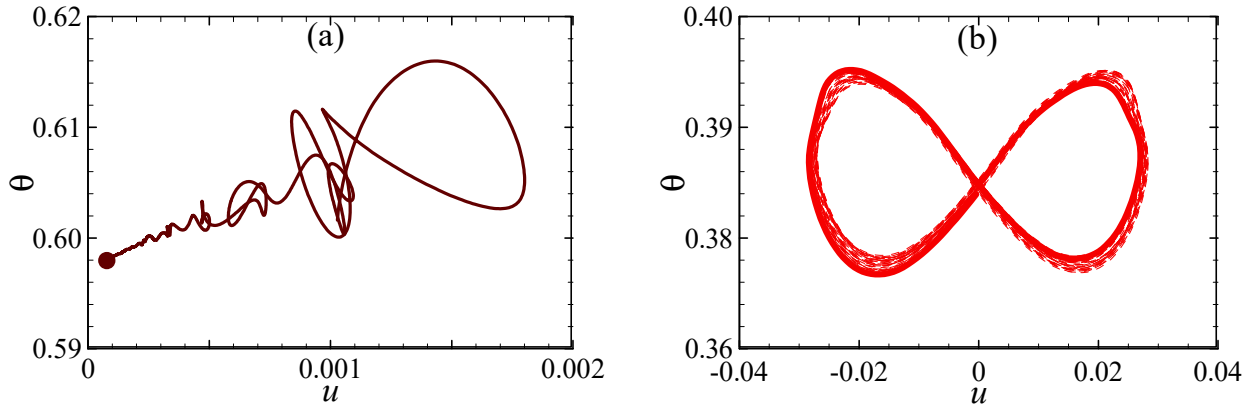

Figure 10. Limit point and limit cycle in the u–θ plane at the point P_4 (0.4, 0.51) for (**a**) Ra = 10^6 and (**b**) Ra = 10^7.

At point P_3 (0, 0.8) for Ra = 10^7 and 10^8, the directions of the phase space of the u–θ plane are depicted in Figure 11 with a view to demonstrating the transformation to chaotic from the periodic condition in greater detail. In Figure 11a, the limit cycle can be seen, indicating that the unsteady flow is periodic for Ra = 10^7, which is compatible with Figure 9. In Figure 11b, the trajectory turns out to be chaotic for Ra = 10^8, indicating that the periodic flow transforms into chaotic, which happens within Ra = 10^7 and 10^8. This is referred to [39] for a full description of the phase-space trajectories.

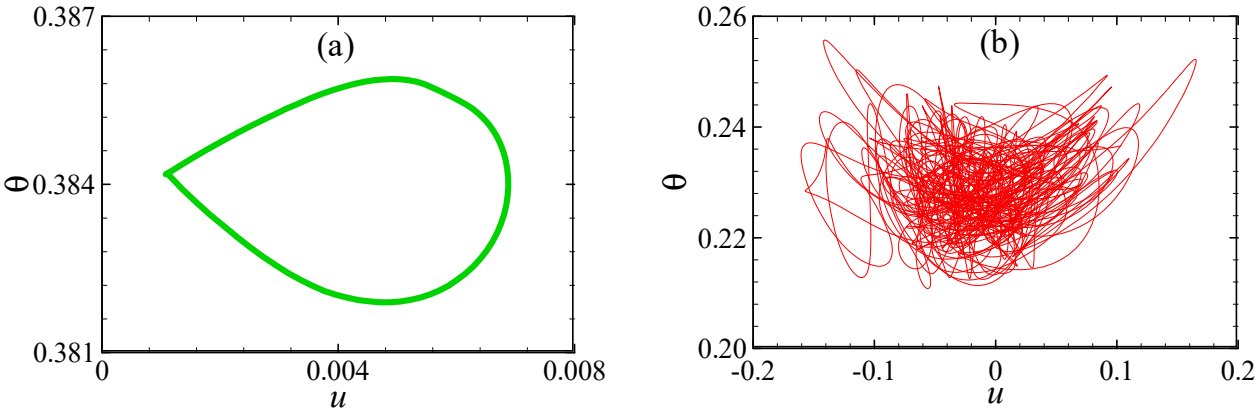

Figure 11. Phase-space trajectories in the u–θ plane at the point P_5 (−0.4, 0.51) for (**a**) Ra = 10^7 and (**b**) Ra = 10^8.

5.2. Impact of Rayleigh Numbers on the Progress of the Flow

An array of Rayleigh numbers, ranging from Ra = 10^3 to 10^8, was used in the simulations. An observation was made in the different transient flow characteristics throughout an array of Rayleigh numbers. For A = 0.5, the isotherms and accompanying streamlines are depicted in Figures 4–7 for different Rayleigh numbers. The numerical findings for the various Rayleigh numbers, as shown in Figure 12, reveal some differences. To begin with, convective flow instabilities can be noticed at the lowermost Rayleigh number. However, with a higher Rayleigh number, the unsteadiness becomes more pronounced, while the

corresponding wave number rises. For Ra = 10^3 to 10^4, the flow is weaker and symmetric behavior is visible, which is expected, i.e., the flow is symmetric and constant. The flow becomes asymmetric for Ra = 10^5 and 10^6 in the transitional stage and becomes steady at the fully developed stage. Lastly, for Ra = 10^7 and Ra = 10^8, the flow becomes periodic and chaotic, respectively.

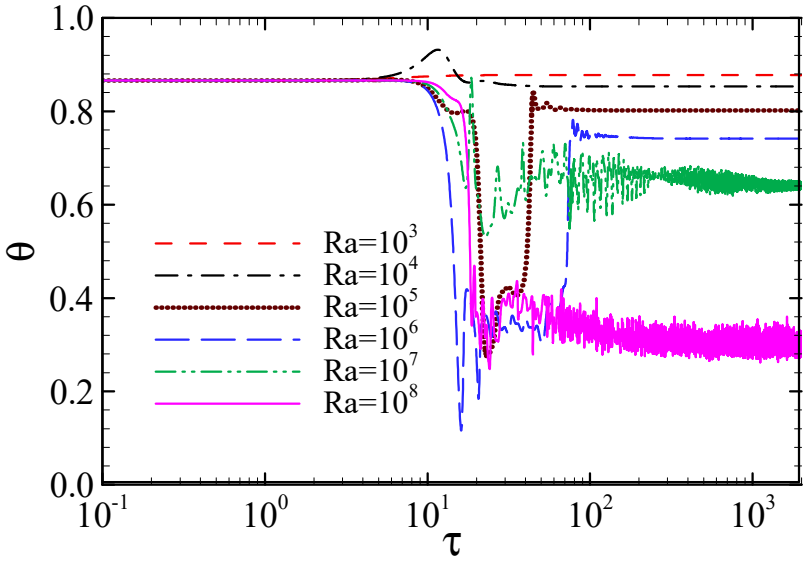

Figure 12. Temperature–time series at point P_1 (0, 0.133) for various Rayleigh numbers.

6. Heat Transfer

The time series of the averaged Nusselt number (Nu) of the lower and upper surfaces were calculated as demonstrated in Figure 13 in order to measure heat transfer through the cavity's wall. In this study, the Nusselt number was defined as follows (Bhowmick et al. [40] and Cui et al. [41]):

$$\mathrm{Nu} = \frac{1}{ln} \int_{ln}^{\frac{d\theta}{dn}} ds. \tag{11}$$

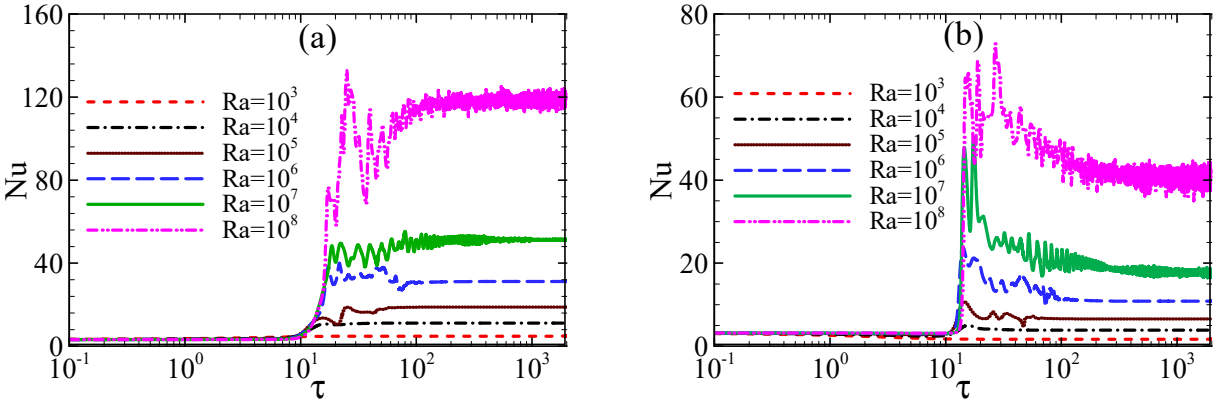

Figure 13. Time series of the Nusselt number for various Ra on (**a**) hot bottom wall and (**b**) cold top wall.

The temperature in the internal cavity changes at various periods in the early stages because the fluid in the cavity is initially stratified. As the upper and lower walls are cooled and heated at the same time, due to the initially stratified fluid, no significant distinction in temperature between the fluid observed, and the wall might lead to tiny heat transfer; as a result, a small Nu value is predicted initially. The stratification breaks down with time,

and the temperature differential in the interior cavity approaches zero. When the fluid's stratification becomes weaker, then the waviness of Nu is increased with increased Ra. In the transitional period, for larger Ra, Nu is oscillatory. It is apparent that the Nusselt number on the enclosure's hot bottom wall (Figure 13a) is larger during the transition stage. The cool top wall, however, illustrates the opposite situation (see Figure 13b). At the completely developed stage, the Nusselt number is fixed for $Ra \leq 10^6$ and oscillatory for $Ra \geq 10^7$. These findings are compatible with those in Figure 12.

7. Conclusions

This study was concerned with the transient thermal convection in a trapezoidal cavity stuffed with linearly stratified air. Although the inclined walls remained adiabatic, the base wall was warmed, and the top wall was cooled with a specified aspect ratio $A = 0.5$ with variation of Ra (10^0 to 10^8). The finite volume-based FLUENT software was used to conduct the numerical simulation. The key findings of this study are described below.

According to numerical simulation, the development of transient flow within the enclosure owing to the predefined boundary conditions could be categorized into three separate stages: early, transitional, and steady or unsteady, all of which were shown in Figures 4–7.

The flow at the beginning phase was portrayed through the arrangement of thermal boundary layers close toward every internal surface and the commencement of primary circulations. In the energy conditions, whenever the terms of convection and conduction were adjusted, the flow went into the transitional state. In the transitional level, the flow was depicted via the base of convective dangers through ascending and descending thermal plumes, as well as the creation of the cellular flow formations. Furthermore, symmetric flows regarding the geometrically symmetric plane for smaller Ra, as well as for relatively higher Ra, were characterized by pitchfork bifurcation, representing the flow from symmetry to asymmetry. With respect to the variance in Ra, the timescale for the flow development was likewise computed. For the pitchfork bifurcation, the difference in the behavior of symmetric and asymmetric flow was additionally examined.

For the stratified air, the temperatures of the fluid adjacent to the top and base walls were the same as the temperature of the walls. Heat transmission was studied through the enclosure, as well as at the base and top walls, and it was discovered that, initially, the Nu was small for the stratified air, whereas, after stratification breakup, Nu gradually increased in the transitional stage, and it was fixed for $Ra \leq 10^6$ and oscillatory for $Ra \geq 10^7$ at the completely developed stage. Moreover, on the basis of the numerical results, the heat transmission was measured, and it was shown that the Nusselt number depends on the Rayleigh number.

Author Contributions: Conceptualization, S.C.S. and S.B.; methodology, M.M.R. and S.B.; validation, M.M.R. and S.B.; formal analysis, M.M.R., S.B., S.C.S.; investigation, M.M.R. and S.B.; writing—original draft preparation, M.M.R.; writing—review and editing, S.C.S., S.B. and R.N.M.; visualization, M.M.R.; supervision, S.B. and R.N.M.; project administration, S.B. All authors have read and agreed to the published version of the manuscript.

Funding: This research received no external funding.

Data Availability Statement: All data produced from the simulations are used in this manuscript.

Conflicts of Interest: The authors declare no conflict of interest.

Nomenclature

A	aspect ratio
g	gravitational force (m/s^2)
L, H	half-length and height of the enclosure (m)
ln	dimensionless length of the horizontal wall
n	dimensionless coordinate normal to the horizontal wall
s	dimensionless coordinate along the horizontal wall
t	time (s)
P	Pressure (N/m^2)
Nu	Nusselt number
Pr	Prandtl number
Ra	Rayleigh number, $g\beta(T_h - T_c)H^3/\nu\kappa$
T	dimensional temperature (K)
T_∞	dimensional ambient temperature (K)
T_h	dimensional temperature of the heated bottom wall (K)
T_c	dimensional temperature of the cooled top wall (K)
ΔT	temperature difference, $(T_h - T_c)$
u, v	dimensional velocity components (m/s)
U, V	dimensionless velocity components
x, y	dimensional horizontal and vertical coordinates
X, Y	dimensionless horizontal and vertical coordinates
β	thermal expansion coefficient (1/K)
κ	thermal diffusivity (m^2/s)
ν	kinematic viscosity (m^2/s)
ρ	density (kg/m^3)
τ	dimensionless time
$\Delta\tau$	dimensionless timestep
θ	dimensionless temperature

References

1. Patterson, J.; Imberger, J. Unsteady natural convection in a rectangular cavity. *J. Fluid Mech.* **1980**, *100*, 65–86. [CrossRef]
2. Kuhn, D.; Oosthuizen, P.H. Unsteady natural convection in a partially heated rectangular cavity. *J. Heat Transfer.* **1987**, *109*, 798–801. [CrossRef]
3. Ma, J.; Xu, F. Unsteady natural convection and heat transfer in a differentially heated cavity with a fin for high Rayleigh numbers. *Appl. Therm. Eng.* **2016**, *99*, 625–634. [CrossRef]
4. Wen, X.; Wang, L.-P.; Guo, Z. Development of unsteady natural convection in a square cavity under large temperature difference. *Phys. Fluids* **2021**, *33*, 084108. [CrossRef]
5. Saha, S.C. Unsteady natural convection in a triangular enclosure under isothermal heating. *Energy Build.* **2011**, *43*, 695–703. [CrossRef]
6. Lei, C.; Armfield, S.W.; Patterson, J.C. Unsteady natural convection in a water-filled isosceles triangular enclosure heated from below. *Int. J. Heat Mass Transf.* **2008**, *51*, 2637–2650. [CrossRef]
7. Saha, S.C.; Patterson, J.C.; Lei, C. Natural convection and heat transfer in attics subject to periodic thermal forcing. *Int. J. Therm. Sci.* **2010**, *49*, 1899–1910. [CrossRef]
8. Saha, S.C.; Patterson, J.C.; Lei, C. Natural convection in attics subject to instantaneous and ramp cooling boundary conditions. *Energy Build.* **2010**, *42*, 1192–1204. [CrossRef]
9. Bhowmick, S.; Saha, S.C.; Qiao, M.; Xu, F. Transition to a chaotic flow in a V-shaped triangular cavity heated from below. *Int. J. Heat Mass Transf.* **2019**, *128*, 76–86. [CrossRef]
10. Bhowmick, S.; Xu, F.; Molla, M.M.; Saha, S.C. Chaotic phenomena of natural convection for water in a V-shaped enclosure. *Int. J. Therm. Sci.* **2022**, *176*, 107526. [CrossRef]
11. Wang, X.; Bhowmick, S.; Tian, Z.F.; Saha, S.C.; Xu, F. Experimental study of natural convection in a V-shape-section cavity. *Phys. Fluids* **2021**, *33*, 014104. [CrossRef]
12. Iyican, L.; Bayazitoglu, Y.; Witte, L.C. An analytical study of natural convective heat transfer within a trapezoidal enclosure. *J. Heat Transf.* **1980**, *102*, 640–647. [CrossRef]
13. Iyican, L.; Witte, L.C.; Bayazitoglu, Y. An Experimental Study of Natural Convection in Trapezoidal Enclosures. *J. Heat Transf.* **1980**, *102*, 648–653. [CrossRef]
14. Lee, T. Computational and experimental studies of convective fluid motion and heat transfer in inclined non-rectangular enclosures. *Int. J. Heat Fluid Flow* **1984**, *5*, 29–36. [CrossRef]
15. Lam, S.W.; Gani, R.; Symons, J.G. Experimental and Numerical Studies of Natural Convection in Trapezoidal Cavities. *J. Heat Transf.* **1989**, *111*, 372–377. [CrossRef]

16. Lee, T.S. Mixed laminar heat and fluid flow in flow-through opened trapezoidal cooling chambers of low aspect ratios. *Int. J. Numer. Methods Heat Fluid Flow* **1991**, *1*, 31–49. [CrossRef]
17. Lee, T.S. Numerical experiments with fluid convection in tilted nonrectangular enclosures. *Numer. Heat Transfer Part A Appl.* **1991**, *19*, 487–499. [CrossRef]
18. Perić, M. Natural Convection in Trapezoidal Cavities. *Numer. Heat Transf. Part A Appl.* **1993**, *24*, 213–219. [CrossRef]
19. Sadat, H.; Salagnac, P. Further results for laminar natural convection in a two-dimensional trapezoidal enclosure. *Numer. Heat Transf. Part A Appl.* **1995**, *27*, 451–459. [CrossRef]
20. Kuyper, R.A.; Hoogendoorn, C.J. Laminar natural convection flow in trapezoidal enclosures. *Numer. Heat Transfer Part A Appl.* **1995**, *28*, 55–67. [CrossRef]
21. Boussaid, M.; Djerrada, A.; Bouhadef, M. Thermosolutal transfer within trapezoidal cavity. *Numer. Heat Transfer, Part A Appl.* **2003**, *43*, 431–448. [CrossRef]
22. Moukalled, F.; Darwish, M. Natural Convection in a Trapezoidal Enclosure Heated from the Side with a Baffle Mounted on Its Upper Inclined Surface. *Heat Transf. Eng.* **2004**, *25*, 80–93. [CrossRef]
23. Natarajan, E.; Roy, S.; Basak, T. Effect of Various Thermal Boundary Conditions on Natural Convection in a Trapezoidal Cavity with Linearly Heated Side Wall(s). *Numer. Heat Transfer, Part B Fundam.* **2007**, *52*, 551–568. [CrossRef]
24. Hammami, M.; Mseddi, M.; Baccar, M. Numerical study of coupled heat and mass transfer in a trapezoidal cavity. *Eng. Appl. Comput. Fluid Mech.* **2007**, *1*, 216–226. [CrossRef]
25. Natarajan, E.; Basak, T.; Roy, S.J. Natural convection flows in a trapezoidal enclosure with uniform and non-uniform heating of bottom wall. *Int. J. Heat Mass Transf.* **2008**, *51*, 747–756. [CrossRef]
26. Basak, T.; Roy, S.; Pop, I. Heat flow analysis for natural convection within trapezoidal enclosures based on heat line concept. *Int. J. Heat Mass Transf.* **2009**, *52*, 2471–2483. [CrossRef]
27. Tracy, N.I.; Crunkleton, D.W. Oscillatory natural convection in trapezoidal enclosures. *Int. J. Heat Mass Transf.* **2012**, *55*, 4498–4510. [CrossRef]
28. Mustafa, A.W.; Ghani, I.A. Natural convection in trapezoidal enclosure heated partially from below. *Al-Khwarizmi Eng. J.* **2012**, *8*, 76–85.
29. da Silva, A.; Fontana, E.; Mariani, V.C.; Marcondes, F. Numerical investigation of several physical and geometric parameters in the natural convection into trapezoidal cavities. *Int. J. Heat Mass Transf.* **2012**, *55*, 6808–6818. [CrossRef]
30. Gholizadeh, M.M.; Nikbakhti, R.; Khodakhah, J.; Ghasemi, A. Numerical study of double diffusive buoyancy forces induced natural convection in a trapezoidal enclosure partially heated from the right sidewall. *Alex. Eng. J.* **2016**, *55*, 779–795. [CrossRef]
31. Yazdani, K.; Sahebjamei, M.; Ahmadpour, A. Natural convection heat transfer and entropy generation in a porous trapezoidal enclosure saturated with power-law non-Newtonian fluids. *Heat Transf. Eng.* **2020**, *41*, 982–1001. [CrossRef]
32. Gowda, K.G.B.M.; Rajagopal, M.S.; Aswatha; Seethramu, K.N. Numerical Studies on Natural Convection in a Trapezoidal Enclosure with Discrete Heating. *Heat Transf. Eng.* **2019**, *41*, 595–606. [CrossRef]
33. Saha, S.C.; Khan, M. A review of natural convection and heat transfer in attic-shaped space. *Energy Build.* **2011**, *43*, 2564–2571. [CrossRef]
34. Armfield, S.; Street, R. The Fractional-Step Method for the Navier–Stokes Equations on Staggered Grids: The Accuracy of Three Variations. *J. Comput. Phys.* **1999**, *153*, 660–665. [CrossRef]
35. Armfield, S.; Street, R. An analysis and comparison of the time accuracy of fractional-step methods for the Navier-Stokes equations on staggered grids. *Int. J. Numer. Methods Fluids* **2002**, *38*, 255–282. [CrossRef]
36. Armfield, S.; Street, R. A comparison of staggered and non-staggered grid Navier–Stokes solutions for the 8:1 cavity natural convection flow. *ANZIAM J.* **2004**, *46*, C918–C934. [CrossRef]
37. Leonard, B.P.; Mokhtari, S. *ULTRA-SHARP Non-oscillatory Convection Schemes for High-Speed Steady Multidimensional Flow, NASA TM 1-2568 (ICOMP-90-12)*; NASA Lewis Research Centre: Sandusky, OH, USA, 1990.
38. Drazin, P.G.; Reid, W.H. *Hydrodynamic Stability*; Cambridge University Press: Cambridge, UK, 2004.
39. McLaughlin, J.B.; Orszag, S.A. Transition from periodic to chaotic thermal convection. *J. Fluid Mech.* **1982**, *122*, 123–142. [CrossRef]
40. Bhowmick, S.; Xu, F.; Zhang, X.; Saha, S.C. Natural convection and heat transfer in a valley shaped cavity filled with initially stratified water. *Int. J. Therm. Sci.* **2018**, *128*, 59–69. [CrossRef]
41. Cui, H.; Xu, F.; Saha, S.C. A three-dimensional simulation of transient natural convection in a triangular cavity. *Int. J. Heat Mass Transf.* **2015**, *85*, 1012–1022. [CrossRef]